

Journal of  
**Applied Remote Sensing**

**Worldwide uncertainty  
assessments of ladar and radar  
signal-to-noise ratio performance  
for diverse low altitude  
atmospheric environments**

Steven T. Fiorino  
Richard J. Bartell  
Matthew J. Krizo  
Gregory L. Caylor  
Kenneth P. Moore  
Thomas R. Harris  
Salvatore J. Cusumano

# Worldwide uncertainty assessments of ladar and radar signal-to-noise ratio performance for diverse low altitude atmospheric environments

Steven T. Fiorino, Richard J. Bartell, Matthew J. Krizo,  
Gregory L. Caylor, Kenneth P. Moore, Thomas R. Harris,  
and Salvatore J. Cusumano

Air Force Institute of Technology, Center for Directed Energy, 2950 Hobson Way,  
Wright-Patterson AFB, OH 45433-7765  
steven.fiorino@afit.edu

**Abstract:** In this study of atmospheric effects on laser ranging and detection (ladar) and radar systems, the parameter space is explored using the Air Force Institute of Technology Center for Directed Energy's (AFIT/CDE) High Energy Laser End-to-End Operational Simulation (HELEEOS) parametric one-on-one engagement level model. The expected performance of ladar systems is assessed at a representative wavelength of 1.557  $\mu\text{m}$  at a number of widely dispersed land and maritime locations worldwide. Radar system performance is assessed at 95 GHz and 250 GHz. Scenarios evaluated include both down looking oblique and vertical engagement geometries over ranges up to 3000 meters in which clear air aerosols and thin layers of fog, locally heavy rain, and low stratus cloud types are expected to occur. Seasonal and boundary layer variations are considered to determine optimum employment techniques to exploit or defeat the environmental conditions. Each atmospheric particulate/obscurant/hydrometeor is evaluated based on its wavelength-dependent forward and off-axis scattering characteristics and absorption effects on system interrogation. Results are presented in the form of worldwide plots of notional signal to noise ratio. The ladar and 95 GHz system types exhibit similar SNR performance for forward oblique clear air operation. 1.557  $\mu\text{m}$  ladar performs well for vertical geometries in the presence of ground fog, but has no near-horizontal performance under such meteorological conditions. It also has no performance if low altitude stratus is present. 95 GHz performs well for both the fog and stratus layer cases, for both vertical and forward oblique geometries. The 250 GHz radar system is heavily impacted by water vapor absorption in all scenarios studied; however it is not as strongly affected by clouds and fog as the 1.557  $\mu\text{m}$  ladar. Locally heavy rain will severely limit ladar system performance at these wavelengths. However, under heavy rain conditions ladar outperforms both radar systems.

**Keywords:** ladar, aerosol extinction, cloud extinction, fog extinction, rain rate effects

## 1 INTRODUCTION

Modeling and simulation can make important direct contributions to the joint warfighting community by helping to establish clear and fully integrated future program requirements. These requirements are best determined via analysis of the expected variability/uncertainty in system performance arising from spatial, spectral and temporal variations in operating conditions. In this study, the HELEEOS modeling and simulation tool, in conjunction with a ladar signal to noise performance model developed by the Sensors Directorate of the Air Force Research Laboratory and a standard version of the radar range equation from the

literature, is used to compare the expected signal to noise ratio performance of ladar and radar systems operating at 1.557  $\mu\text{m}$ , 95 GHz and 250 GHz for a number of widely dispersed land and maritime locations worldwide. The modeling shows that locally heavy rain will greatly limit performance at all frequencies while the rain persists, however ladar does outperform the 95 and 250 GHz radar systems under these conditions. The 1.557  $\mu\text{m}$  system performs well for vertical geometries in the presence of fog, but has no capability through stratus clouds. The 95 GHz radar exhibits good to very good SNR performance for both oblique and vertical paths for both fog and stratus conditions.

### 1.1 HELEEOS Worldwide Seasonal, Diurnal Atmospheric Model

The HELEEOS model, developed by the AFIT Center for Directed Energy under the sponsorship of the High Energy Laser Joint Technology Office was developed to model high energy laser performance during dynamic engagements. Its basic features have been previously described [1]. A key component of HELEEOS is a worldwide probabilistic model of spatial and temporal variations in atmospheric characteristics which has been described in detail [2,3,4]. This atmospheric model spans wavelengths from the visible to radio frequencies. The effects of molecular and aerosol extinction for a set of typical humid, sea level conditions can be seen in the black curve of Fig. 1. Also plotted in Fig. 1 are the additional effects of typical distributions of drops and droplets found in fog, clouds, and rain.

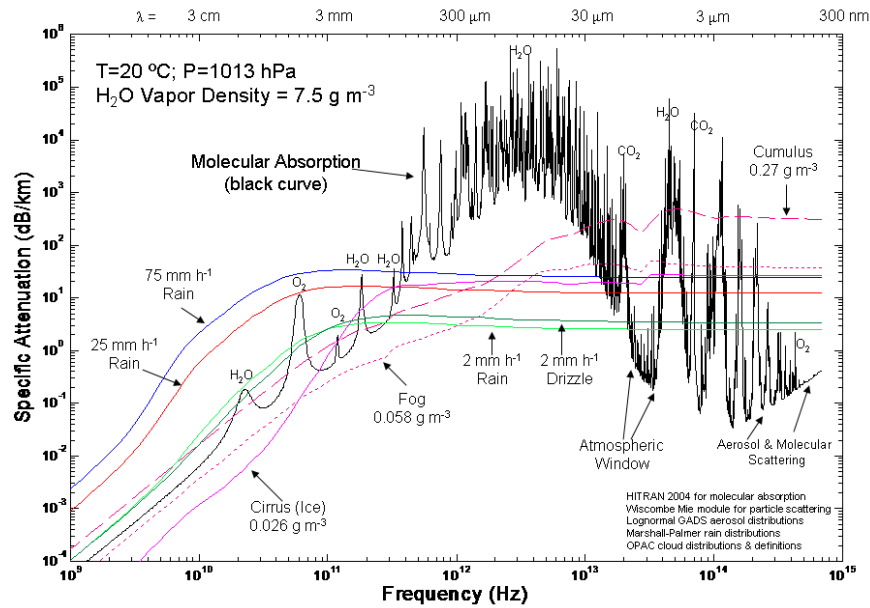


Fig. 1. Specific attenuation from 30 cm to  $\sim 0.4 \mu\text{m}$  (1 GHz to 750 THz). The black line is molecular absorption with some effects of continent average aerosols and molecular scattering included. Colored lines represent the specific attenuation that would be added for the hydrometeor distributions shown (rain, clouds, fog).

## 2 METHODOLOGY

In the current study, the capabilities of the HELEEOS model are exploited to study the worldwide variance in low altitude ladar and radar system performance across a broad range of atmospheric conditions, including the effects of locally heavy rain.

Parameters varied as part of the study:

- 3 wavelengths:
  - 1.557  $\mu\text{m}$ , 1.2 mm (250 GHz), and 3.16 mm (95 GHz)
- 408 ExPERT surface locations worldwide; shown in Fig. 1
- Oceanic locations on a  $1^\circ \times 1^\circ$  latitude/longitude grid, approximately 44000
- Atmospheric conditions:
  - 50<sup>th</sup> percentile relative humidity conditions, i.e. the average RH for each location
  - Daily average for all land sites
  - Variable boundary layer height, dependent upon location
  - Summer and winter seasons
  - Clear sky aerosols
  - Fog, surface to 200 m altitude
  - Low stratus clouds between 500 m and 1000 m altitude
  - Heavy rain, with rate set as a function of location
- Geometry:
  - Air-to-Surface, 1525 m and 3000 m slant ranges
    - Platform altitude 1525 meters
    - Target altitude 0 meters.

## 2.1 System Signal to Noise Ratio

### Ladar

In the current study the impact of variations in atmospheric path transmittance on the signal to noise ratio performance of a hypothetical ladar is assessed. The first step in computing signal to noise ratio is establishing the noise equivalent power (NEP) of this system. Here  $NEP$  is defined:

$$NEP = \frac{hc}{\lambda} \cdot \frac{2B}{\eta} \quad (1)$$

where  $h$  is Planck's constant,  $c$  is the speed of light,  $\lambda$  is the ladar wavelength,  $B$  is the bandwidth, and  $\eta$  is the quantum efficiency. Next, the standard laser radar equation for extended Lambertian targets is applied [5]:

$$P_r = P_s \cdot \frac{D^2}{4R^2} \cdot \rho \cdot T \cdot \eta_t \cdot \eta_r \quad (2)$$

where  $P_r$  is the power received,  $P_s$  is the power transmitted,  $D$  is the aperture diameter (assumed 80 mm),  $R$  is the slant range,  $\rho$  is the optimal reflectivity of 33.33% for targets,  $T$  is the roundtrip atmospheric path transmittance,  $\eta_t$  is the nominal system optics efficiency (here assumed 0.80), and  $\eta_r$  is the nominal receiver optical efficiency, (here assumed 0.80). Finally, signal to noise ratio is computed as the ratio of  $P_r$  to  $NEP$ .

### Radar

For the case of the radar frequencies evaluated as part of the current study, noise energy is computed assuming a matched filter design:

$$noise = k \cdot T_s \cdot F_n \quad (3)$$

Where  $k$  is Boltzmann's constant,  $T_s$  is the system noise temperature, assumed 288K, and  $F_n$  is the noise figure of the receiver, assumed to have a value of 3. The standard radar range equation is applied [6]:

$$signal = \frac{P_{avg} \cdot G^2 \cdot RCS \cdot \lambda^2 \cdot t_{ot} \cdot T}{(4\pi)^3 \cdot R^4} \quad (4)$$

where  $P_{avg}$  is the average power, assumed to be 100 Watts,  $G$  is the gain as a power ratio,  $RCS$  is the radar cross section of the target, assumed here to be 1 m<sup>2</sup>,  $t_{ot}$  is the time on target, assumed to be 10 microseconds,  $R$  is the slant range, and  $T$  is the roundtrip atmospheric path transmittance. Signal to noise ratio is computed as the ratio of these two terms for the radar case.

### 3 RESULTS

Worldwide variations in atmospheric path transmittance were computed and used with the SNR expressions defined above to determine the effect on system SNR.

#### 3.1 Climatology Based Transmittance

Figure 2 compares transmittance across the world for the 3000 m slant range oblique case for 1.557 μm, 95 and 250 GHz for January climatological conditions. A number of observations may be made regarding conditions shown in Fig. 2 for 1.557 μm. Over the northern and southern ocean regions transmittance is reduced due to relative humidity and windspeed driven aerosol effects. Higher wind speeds over ocean areas generate more sea salt aerosols; these aerosols are hygroscopic and tend to become larger as RH approaches 100%. High wind speeds and high RHs combine to create higher aerosol concentrations and larger size distributions over the high ocean latitudes [2]. The land/ocean composite comparisons seen in Fig. 2 and throughout this paper can only be made for 50th percentile relative humidity conditions because only 50th percentile data are currently available for ocean locations. The atmospheric boundary layer thickness for the land sites is 1525 m, while over the ocean it is 500 m [7]. This difference in boundary layer height means that over the oceans a significant portion of the oblique path is located in the free atmosphere above the boundary layer, while over the land the path is entirely within the boundary layer. The free atmosphere is defined in HELEEOS by six different generally latitude-dependent standard atmospheres [2,7]. Each standard or reference atmosphere has a summer and winter variant. Because the 95 and 250 GHz energy is primarily affected by water vapor content, the differences in average absolute humidity among the seasonal standard atmospheres is clearly evident in the over-ocean areas of the bottom plot of Fig. 2. This latitudinal banding due to the free atmosphere definition appears in all subsequent figures with 95 and 250 GHz plots. The latitudinal banding does not appear in the radar plots because the propagation of the shorter wavelength is dominated by site-specific boundary layer effects.

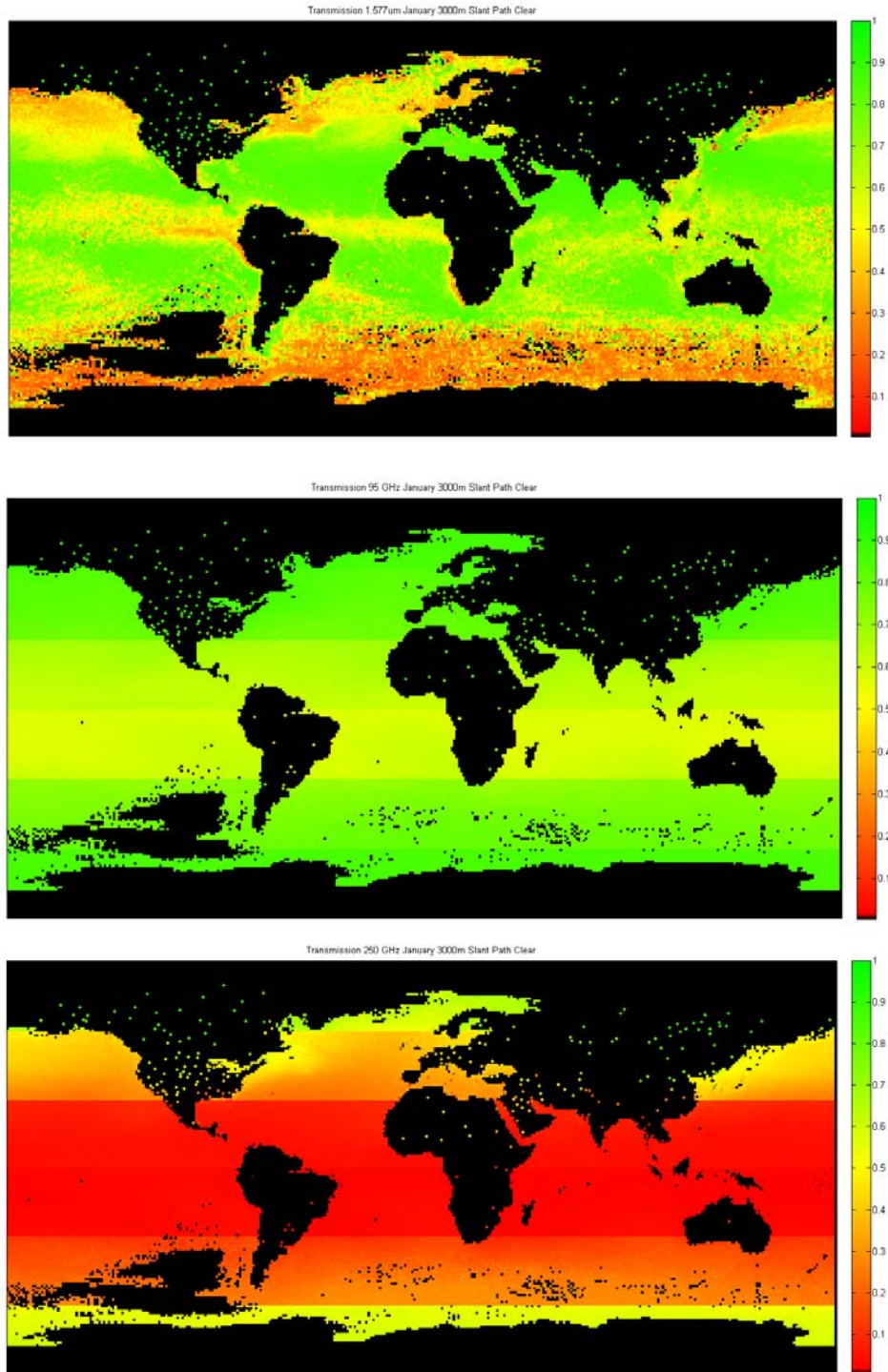


Fig. 2. Worldwide path transmittance values for the climatological atmosphere for 1.557  $\mu\text{m}$  (Top), 95 GHz (Middle), and 250 GHz (Bottom), for January, 50th percentile RH, daily average, molecular and aerosol effects, 3000 m slant range, oblique path, 1525 m platform altitude.

Note in all three plots of Fig. 2, and nearly all subsequent figure plots with over ocean data, that land, ice covered regions, and locations with missing climatological data are depicted as black. The ExPERT land sites appear as color coded dots.

### 3.2 Signal to Noise Ratio Results - Molecular and Aerosol Effects Only

Figure 3 depicts composite worldwide SNR results for all 408 ExPERT land locations and all available oceanic locations at 1.557  $\mu\text{m}$ , 95 and 250 GHz for daily average, 50th percentile relative humidity conditions, for January, for the 3000 meter slant range case. This can be considered the “no cloud, molecular and aerosol effects only” scenario. The simulated 1.557  $\mu\text{m}$  and 95 GHz systems exhibit a similar range of worldwide SNR values for this tactical scenario, with both providing good performance. Referring back to Fig. 2, extinction due to aerosols in the boundary layer strongly impacts 1.557  $\mu\text{m}$ . The results at 95 and 250 GHz, particularly over the ocean, are strongly influenced by the water vapor content of the air. This is especially evident in the tropics. The 250 GHz system is so heavily impacted by water vapor absorption that its performance is significantly less than the other two systems, even in this benign, fair weather scenario. Due to the fact it is least affected by localized aerosol effects, 95 GHz performance tends to be more consistent across broad geographic regions.

Figure 4 depicts composite worldwide SNR results for all 408 ExPERT land locations and all available oceanic locations at 1.557  $\mu\text{m}$ , 95 and 250 GHz for daily average, 50th percentile relative humidity conditions, for January, for the near vertical path case. Performance is improved for all three wavelengths over that of the oblique case of Fig. 3, most markedly for 250 GHz. Because aerosols affect the 1.557  $\mu\text{m}$  propagation more markedly than the radar system wavelengths, the performance at 1.557  $\mu\text{m}$  is least improved in the vertical scenario depicted in Fig. 4 over the oblique scenario in Fig. 3. This is due to the aerosols being mainly confined in the boundary layer (500 m over the oceans and 1524 m over land) which the near vertical path still completely traverses.

Fig. 5 graphically illustrates the seasonal geographic variation in performance for 95 GHz. As can be seen in Fig. 5, conditions are significantly more limiting during each hemisphere’s summer season (southern hemisphere, top; northern hemisphere bottom). This is because summer is generally much warmer than winter, thus allowing the lower atmosphere to contain more water vapor in summer than winter.

### 3.3 Effects of a 200 Meter Fog Layer

Figure 6 depicts composite worldwide SNR results for all 408 ExPERT land locations and all available oceanic locations at 1.557  $\mu\text{m}$ , 95 and 250 GHz for daily average, 50th percentile relative humidity conditions, for January, for 3000 meter slant range oblique case in the presence of 200 m thick fog layer. The conditions in Fig. 7 are identical, except that the path is 1530 m and nearly vertical, given the 1525 m platform altitude.

Performance at 95 GHz for the oblique geometry case in the presence of such a fog layer is similar to that for the no cloud, molecular and aerosol effects only case; as one can see by comparing the middle plot of Fig. 6 to the bottom or top plot in Fig. 5. The 250 GHz performance is also little different from the no cloud, molecular and aerosol effects only case. The 1.557  $\mu\text{m}$  system suffers severe attenuation for this oblique path through fog (note the different color scales in Fig. 6).

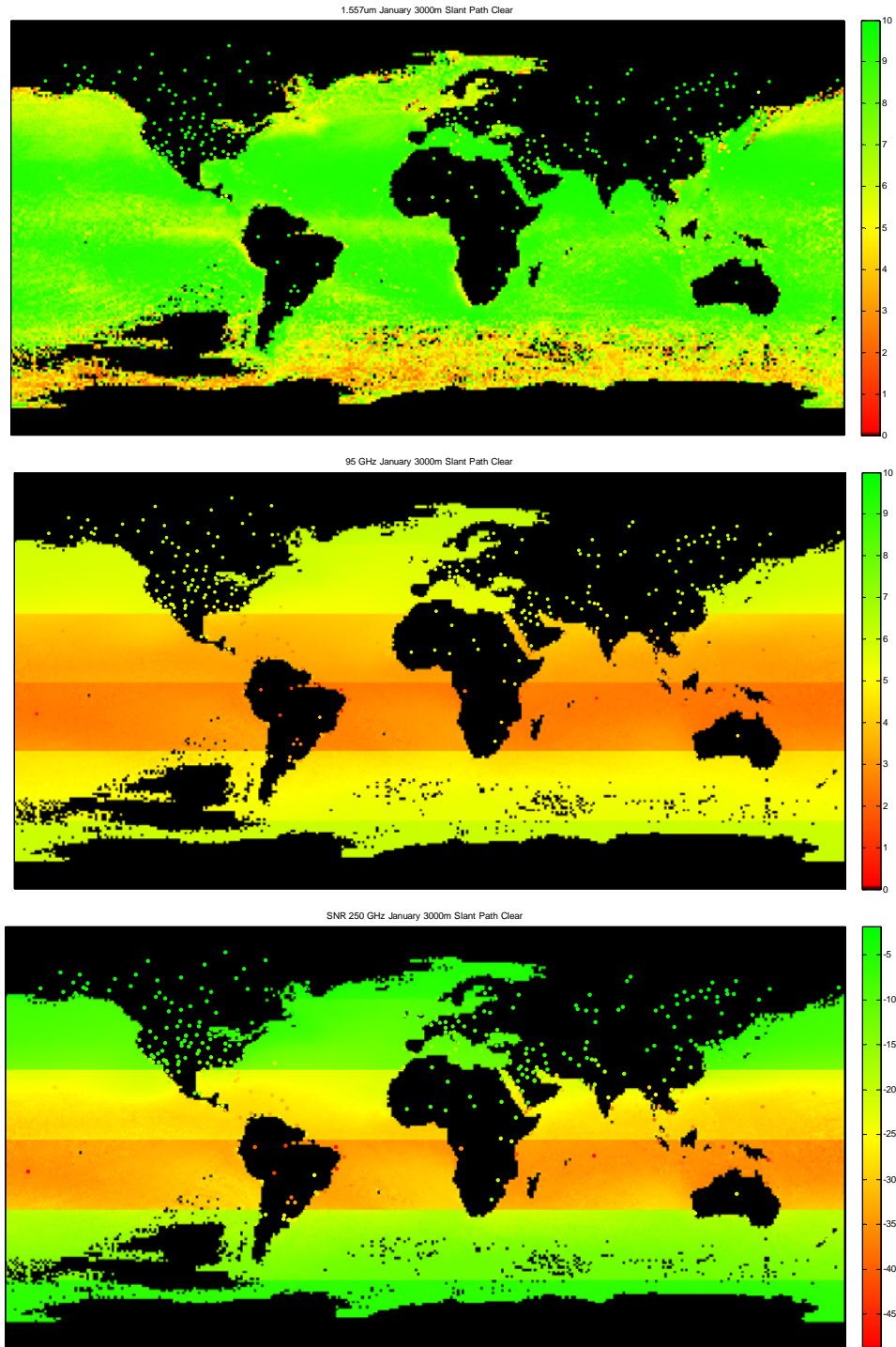


Fig. 3. Worldwide SNR values for 1.557  $\mu\text{m}$  (Top), 95 GHz (Middle), and 250 GHz (Bottom), January, 50th percentile RH, daily average, no cloud, molecular and aerosol effects only, 3000 m slant range, oblique path, 1525 m platform altitude. Note different color scales.

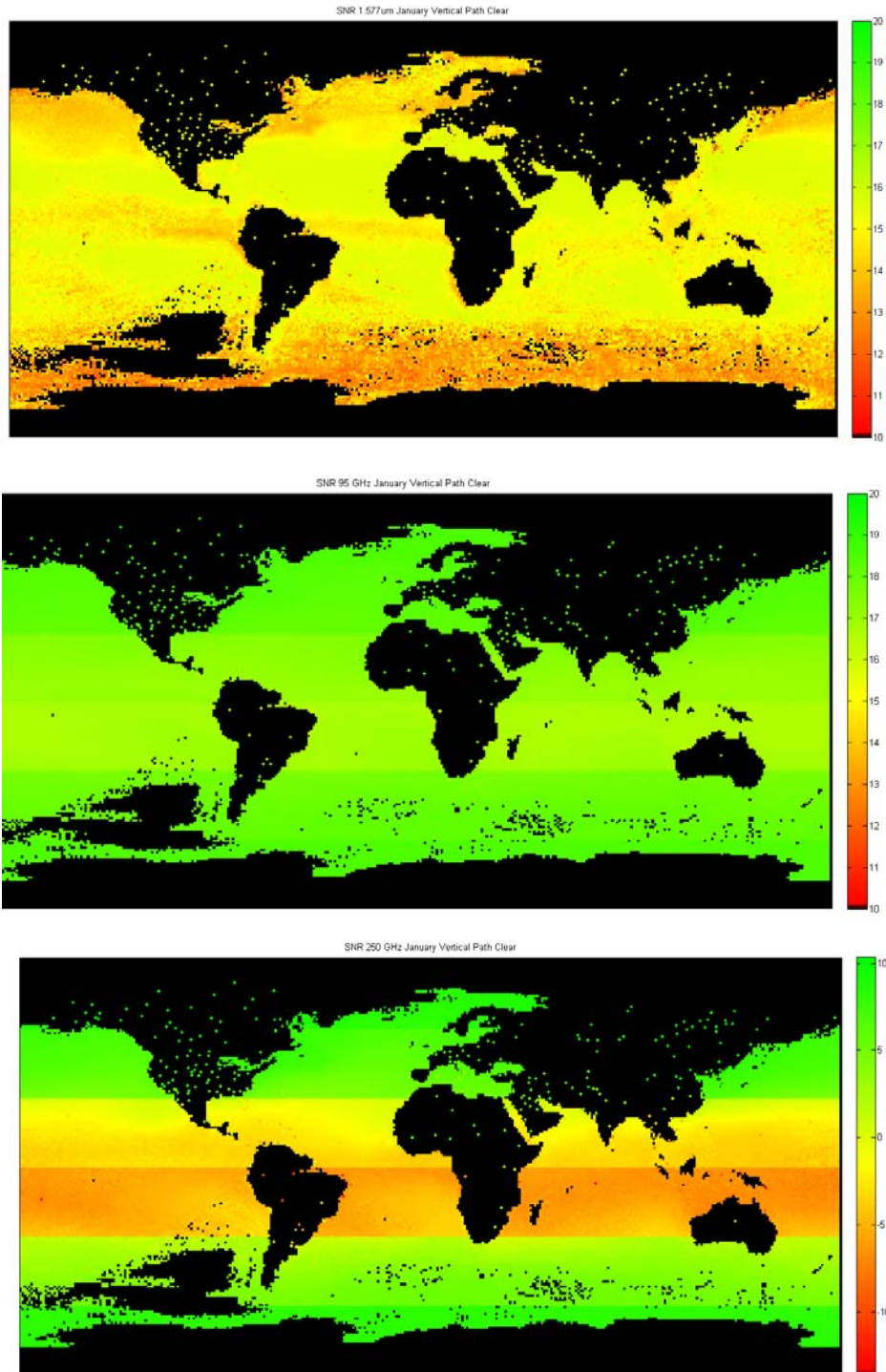


Fig. 4. Worldwide SNR values for 1.557  $\mu\text{m}$  (Top), 95 GHz (Middle), and 250 GHz (Bottom), January, 50th percentile RH, daily average, no cloud, molecular and aerosol effects only, 1530 m slant range, 1525 m platform altitude, near-vertical path. Note different color scales.

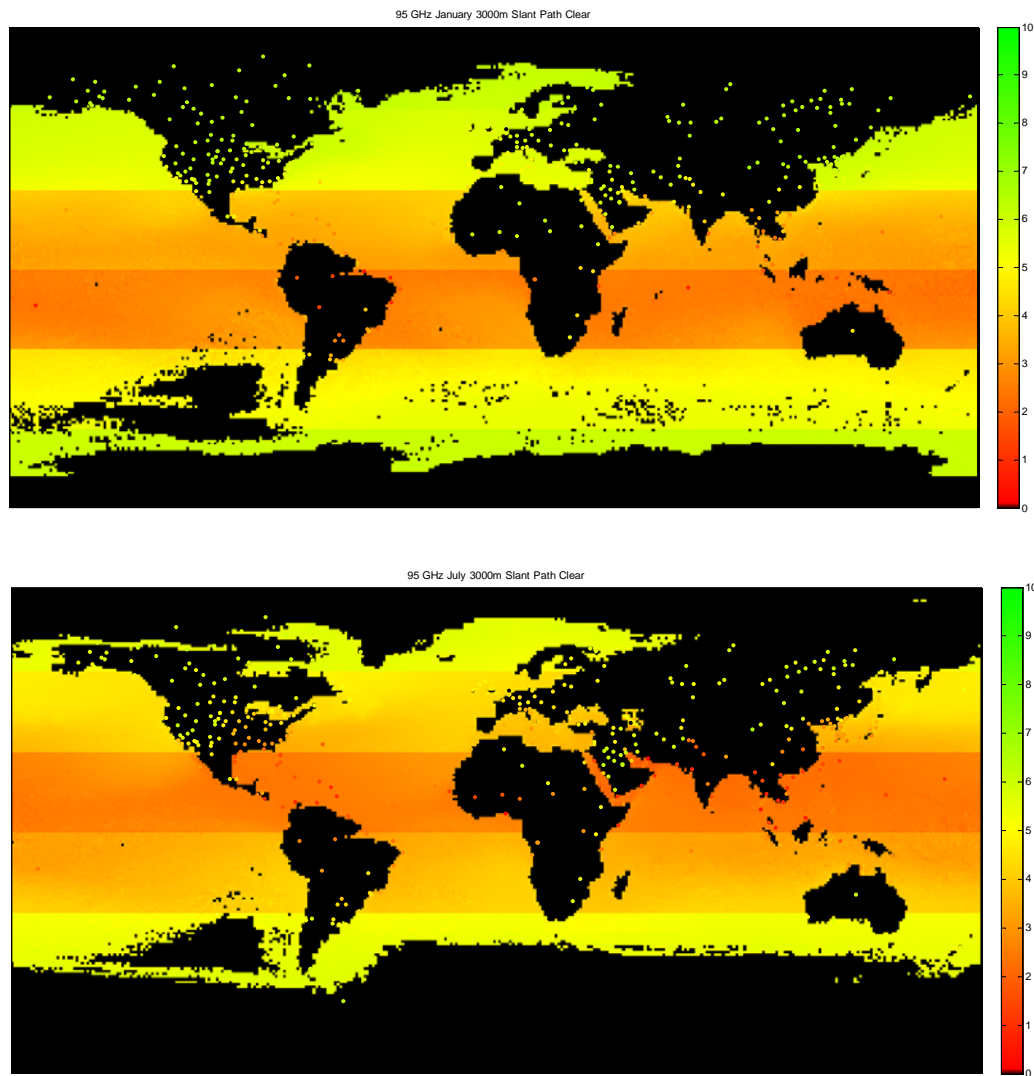


Fig. 5. Comparison of SNR results for 50th percentile RH, daily average, no cloud, molecular and aerosol effects, 3000 m slant range, oblique path, January (Top) and July (Bottom) for 95 GHz, 1525 m platform altitude.

For the near-vertical path case depicted in Fig. 7, 95 GHz achieves very high SNR values worldwide. The performance at 1.557  $\mu\text{m}$  for the near-vertical path through fog is quite similar to its performance for the longer oblique path for the no cloud, molecular and aerosol effects only scenario (Fig. 3, top).

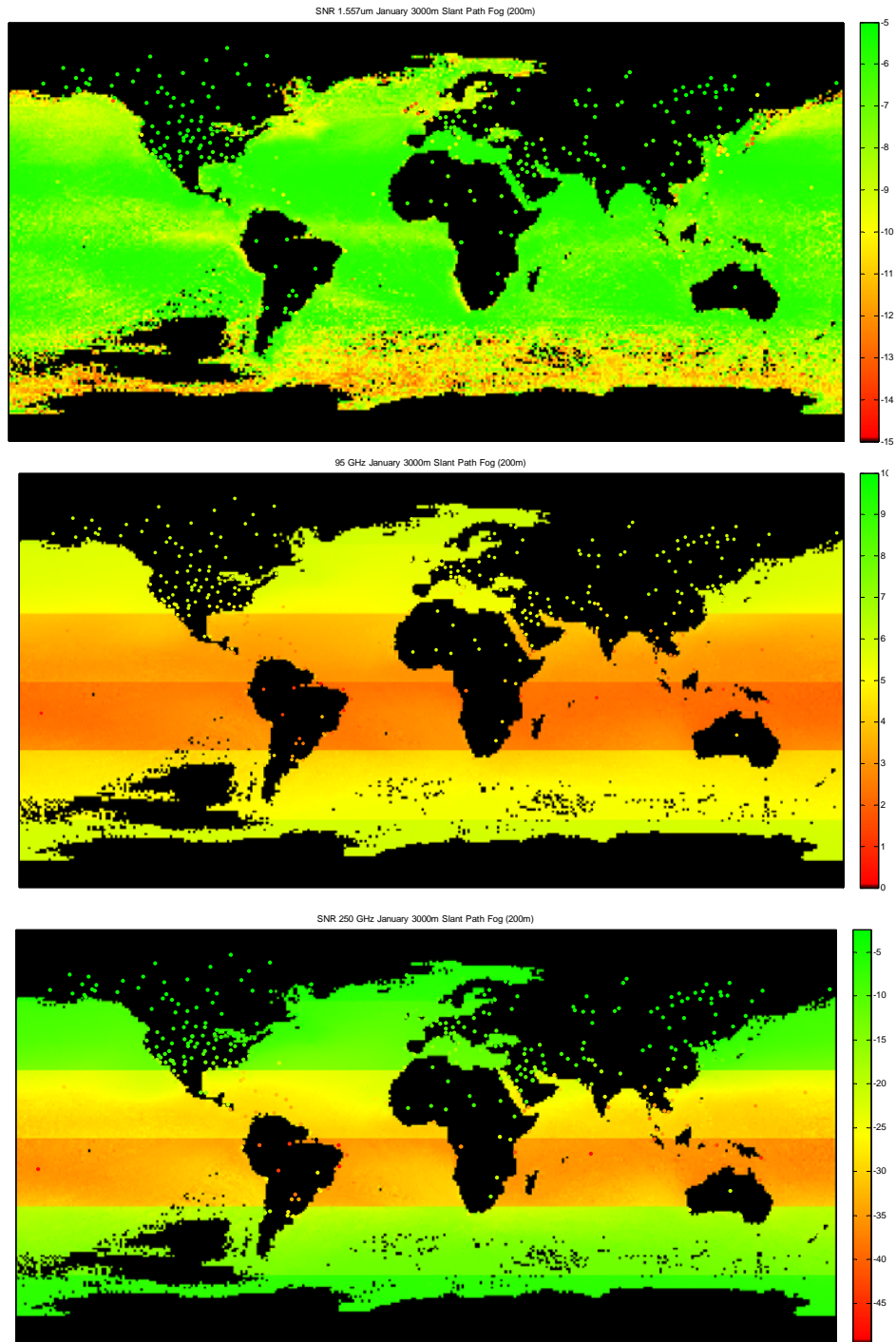


Fig. 6. Worldwide SNR values for 1.557  $\mu\text{m}$  (Top), 95 GHz (Middle), and 250 GHz (Bottom), January, 50th percentile RH, daily average, molecular and aerosol effects plus 200 meter fog layer, 3000 m slant range, oblique path, 1525 m platform altitude. Note different color scales.

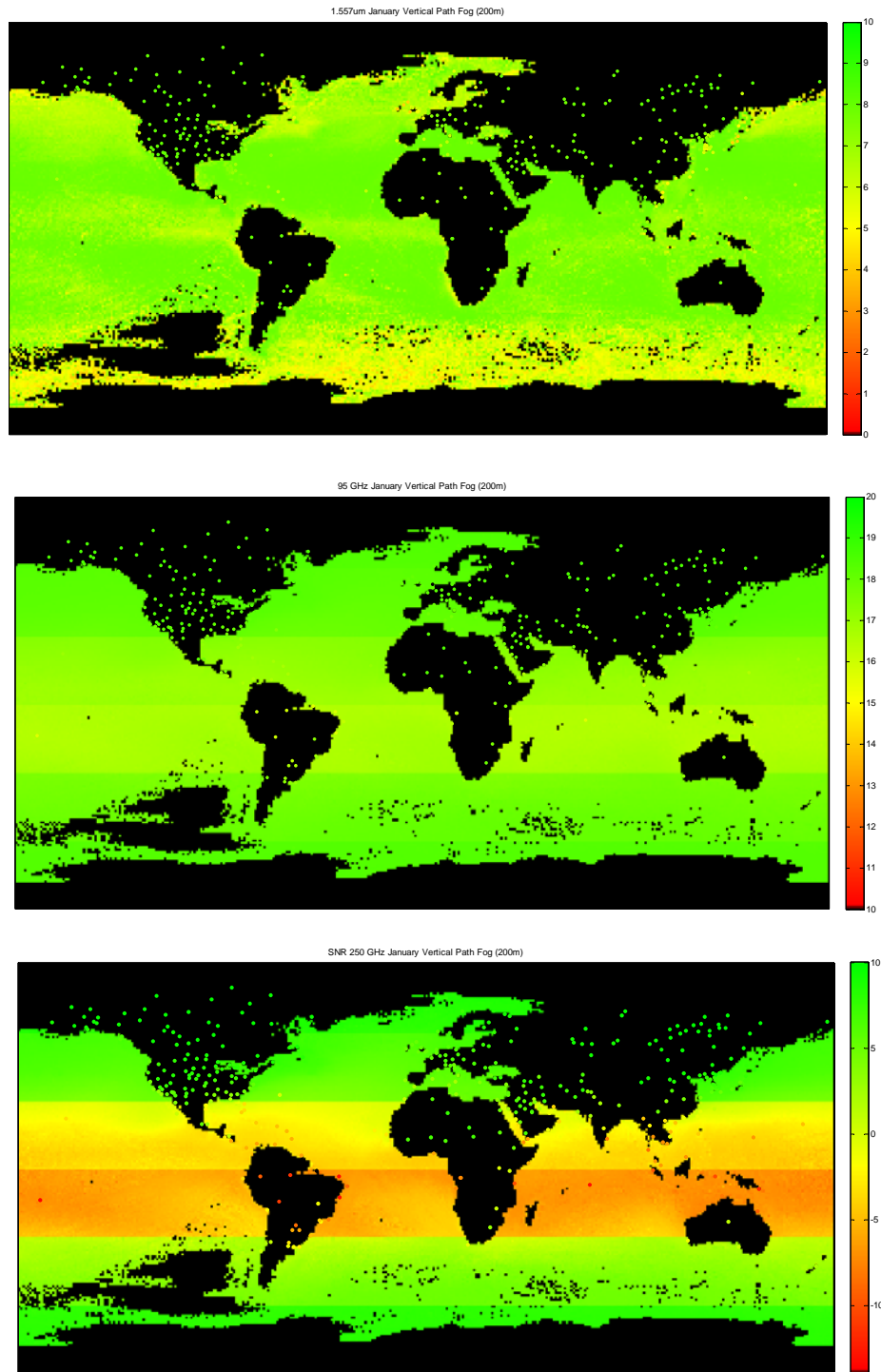
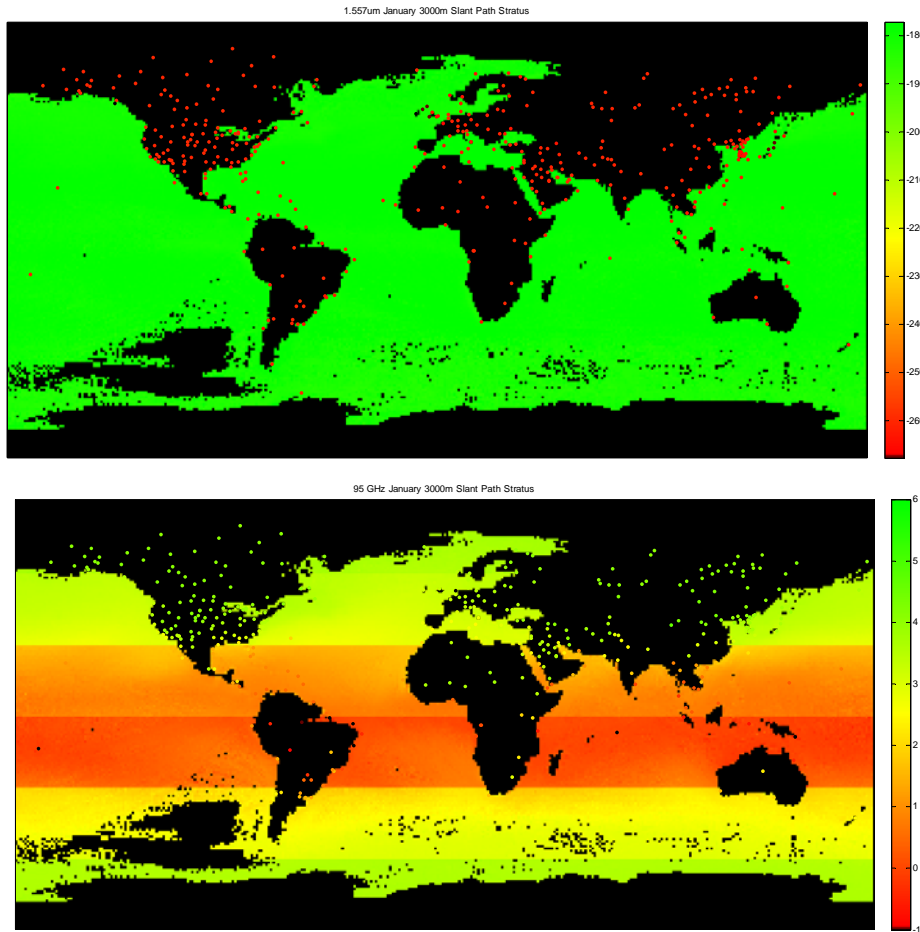


Fig. 7. Worldwide SNR values for 1.557  $\mu\text{m}$  (Top), 95 GHz (Middle), and 250 GHz (Bottom), January, 50th percentile RH, daily average, molecular and aerosol effects plus 200 meter fog layer, 1530 m slant range, 1525 m platform altitude, near-vertical path. Note different color scales.

### 3.4 Effects of a Low Altitude Stratus Layer

Figure 8 depicts composite worldwide SNR results for all 408 ExPERT land locations and all available oceanic locations at 1.557  $\mu\text{m}$ , 95 and 250 GHz for daily average, 50th percentile relative humidity conditions, for January, for 3000 meter slant range oblique case in the presence of a low stratus cloud layer between 500 m and 1000 m above the surface. The conditions in Fig. 9 are identical, except that the path is 1530 m and nearly vertical.

For the both the oblique and near-vertical paths, 1.557  $\mu\text{m}$  ladar system has virtually no capability through such a stratus layer. The 95 GHz system, on the other hand, exhibits good performance under such conditions, only somewhat less than its performance through the 200 m fog layer. The 250 GHz system has very limited capability in the 3000 m path through the stratus layer, but has some usable performance outside of the tropics in the near vertical path, stratus scenario.



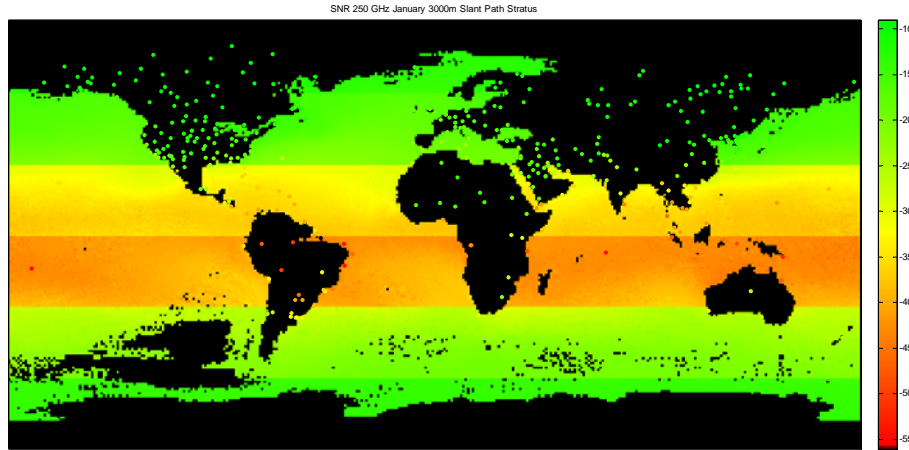
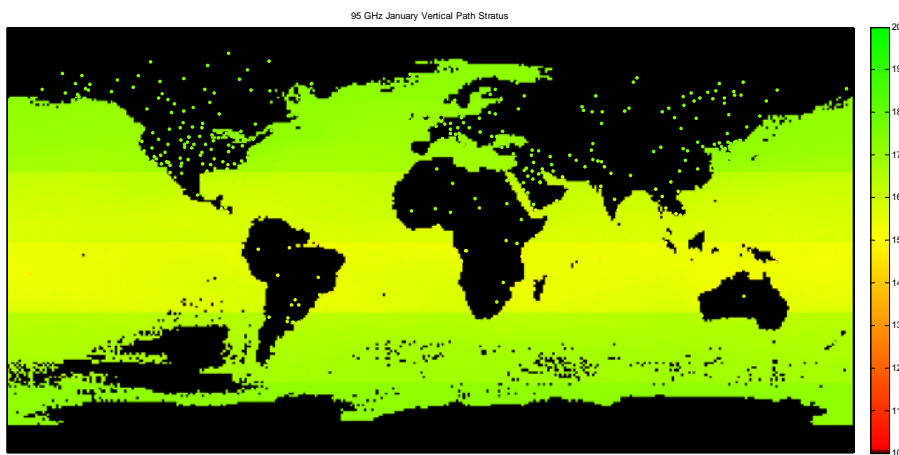
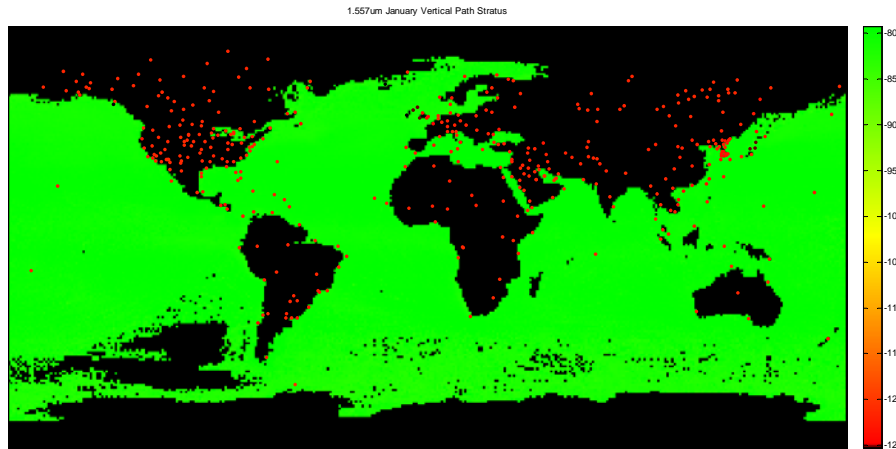


Fig. 8. Worldwide SNR values for 1.557  $\mu\text{m}$  (Top), 95 GHz (Middle), and 250 GHz (Bottom), January, 50th percentile RH, daily average, molecular and aerosol effects plus stratus layer between 500 m and 1000 m, 3000 m slant range, oblique path, 1525 m platform altitude. Note different color scales.



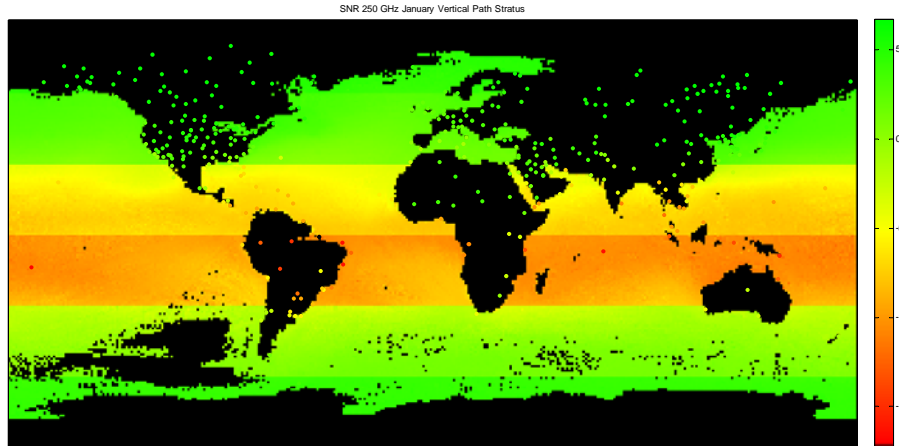


Fig. 9. Worldwide SNR values for 1.557  $\mu\text{m}$  (Top), 95 GHz (Middle), and 250 GHz (Bottom), January, 50th percentile RH, daily average, molecular and aerosol effects plus stratus layer between 500 m and 1000 m, 1530 m slant range, near-vertical path, 1525 m platform altitude. Note different color scales.

### 3.5 Effects of Location-Dependent Heavy Rain

HELEEOS includes a tool for summarizing probability of rain rate as a function of location, as well as the capability to predict the effect of any specific rain rate on path extinction for any wavelength. The rain rate climatology used in HELEEOS follows that of Crane and Blood [8].

Figure 10 depicts 99.98th percentile rain rates, in  $\text{mm h}^{-1}$ , for the entire world, corresponding to locally heavy rain. There is significant variation worldwide, with the heaviest rain rates expected in the tropical regions. These are tabulated on a yearly basis, in most locations these rates correspond to summer conditions. Thus, the 99.98th percentile corresponds to 0.02 percent of the year, or about 1.75 hours per year total. The 0.02 percent threshold was chosen because it is in the middle of the range of “percent of year” values computed for the original Crane and Blood study. The minimum heavy rain rate at the 99.98th percentile level is  $12 \text{ mm h}^{-1}$  and the maximum is  $115 \text{ mm h}^{-1}$  [2].

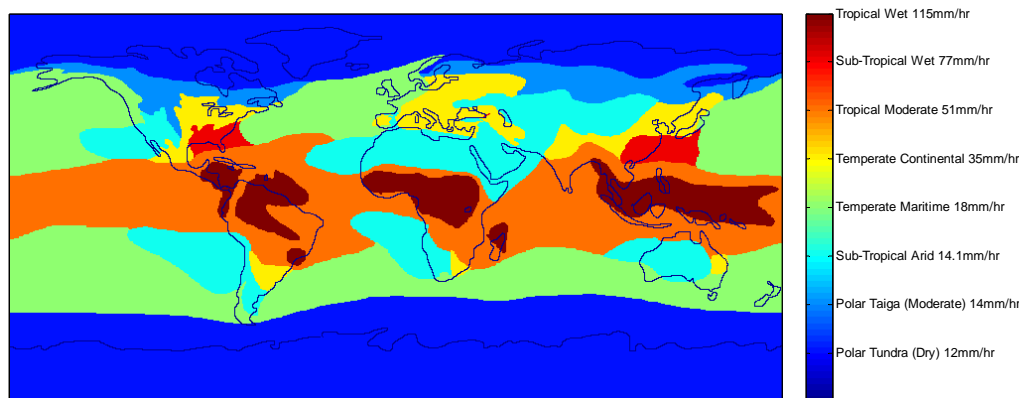


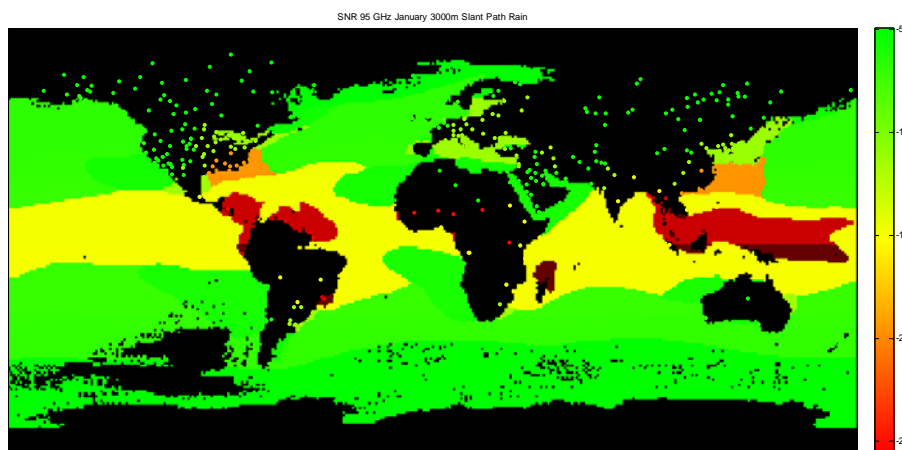
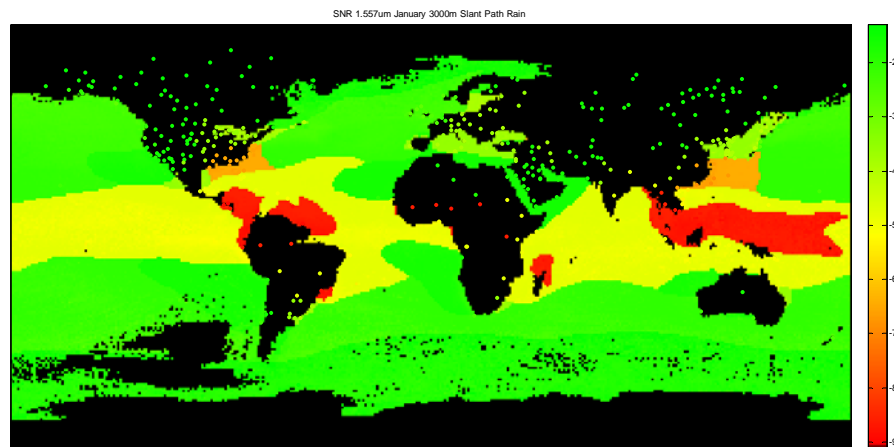
Fig. 10. 99.98th percentile rain rate ( $\text{mm h}^{-1}$ ) worldwide.

Figure 11 summarizes composite worldwide SNR results for all 408 ExPERT land locations and all available oceanic locations at 1.557  $\mu\text{m}$ , 95 and 250 GHz for daily average, 50th

percentile relative humidity conditions, for January, for 3000 meter slant range oblique case in the presence of locally extremely heavy rate, with the location-specific rate set as indicated in Fig. 10. Platform altitude is 1525 m in Fig. 11, with no clouds along the slant path.

As one might expect for a ladar system operating at 1 to 2  $\mu\text{m}$  wavelength, SNR values are low in heavy rain rate scenarios. However, the ladar system does outperform the 95 and 250 GHz radar systems under these conditions. This is due to the rain drop size distribution containing a significant number of drops that are very nearly the same size as the sub-millimeter to millimeter wavelengths of the radars. This puts the radar energy close to the Mie resonance region for scattering effects, thus increasing the extinction over the shorter wavelength, as is evidenced by the slight increase in specific attenuation due the various rain rates shown in Fig. 10. Furthermore, liquid water is slightly more absorbing of sub-millimeter to millimeter wavelength energy than it is of energy at 1 to 2  $\mu\text{m}$ .

In the near-vertical heavy rain scenarios (not shown), the ladar performance at 1.557  $\mu\text{m}$  is only modestly degraded relative to the near-vertical no clouds, aerosols only case—at locations where climatologically “heavy rain” is less than  $\sim 20 \text{ mm h}^{-1}$ . These lighter heavy rain areas correspond to the blue and green shaded regions in Fig. 10. The performance at the radar wavelengths in the near-vertical heavy rain scenarios is degraded significantly relative to the near-vertical no clouds, aerosols only case at all geographic locations.



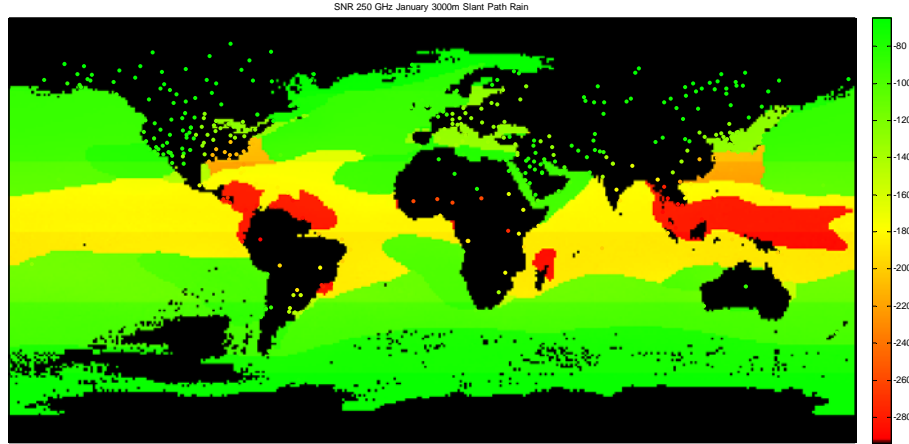


Fig. 11. Worldwide SNR values for 1.557  $\mu\text{m}$  (Top), 95 GHz (Middle), and 250 GHz (Bottom), January, 50th percentile RH, daily average, molecular and aerosol effects, plus locally heavy rain (99.98th percentile), 3000 m slant range, 1525 m platform altitude. Note different color scales.

#### 4 SUMMARY

Effects of using geographic location and seasonal climatological data in determination of lidar and radar SNR have been analyzed. In the absence of clouds and precipitation, aerosols are the primary attenuator of 1 to 2  $\mu\text{m}$  lidar SNR performance in scenarios traversing the atmospheric boundary layer. These aerosols are in general modified by relative humidity, thus causing boundary layer lidar SNR to be highly sensitive to location and season. The 95 and 250 GHz radar SNRs are dominated by effects of the water vapor content of the air; in general they perform better in less humid winter scenarios.

Both the simulated 1.557  $\mu\text{m}$  lidar and the simulated 95 GHz radar systems perform well in the no cloud, molecular and aerosol effects only scenario. The 250 GHz radar is so strongly affected by water vapor absorption, especially in the humid tropics, that its performance suffers in comparison to the other two systems in the no cloud, molecular and aerosol effects only scenario.

The simulated 1.557  $\mu\text{m}$  lidar performs adequately for near-vertical geometries in the presence of a ground fog layer, but has no forward looking oblique performance under such meteorological conditions. It also has no performance if low altitude stratus clouds are present. The simulated 95 GHz radar system, on the other hand, performs well for both the fog and stratus layer cases, for both vertical and forward oblique geometries. The 250 GHz radar is not strongly affected by the fog or cloud scenarios, however its usability in these cases is limited to areas outside the tropics due to humidity. Radar is clearly the choice in the presence of clouds and fog. These relative impacts on expected system performance, as compared to the clear sky, molecular and aerosol effects only scenario, are summarized in Table 1 for the oblique geometry case, and in Table 2 for the near-vertical geometry case.

Locally heavy rain will severely limit lidar and radar system performance at the wavelengths studied during the period of time such rain fall persists. However, under cloud-free heavy rain conditions, 1 to 2  $\mu\text{m}$  lidar outperforms sub-millimeter to millimeter wavelength radar.

Table 1. Summary of the relative effect of the atmospheric conditions analyzed on expected system performance, oblique geometry, relative to the clear sky/molecular and aerosol effects only case.

	1.557 $\mu\text{m}$	95 GHz	250 GHz
Fog	significant	minimal	minimal
Stratus	significant	minimal	modest
Locally heavy rain	significant	significant	significant

Table 2. Summary of the relative effect of the atmospheric conditions analyzed on expected system performance, near vertical geometry, relative to the clear sky/molecular and aerosol effects only case.

	1.557 $\mu\text{m}$	95 GHz	250 GHz
Fog	modest	minimal	minimal
Stratus	significant	minimal	modest
Locally heavy rain	modest to significant	significant	significant

### Acknowledgments

The authors recognize the outstanding support of the High Energy Laser Joint Technology Office, Albuquerque, New Mexico. The views expressed in this paper are those of the authors and do not necessarily reflect the official policy or position of the Air Force, the Department of Defense or the U.S. Government.

### References

- [1] R. J. Bartell, G. P. Perram, S. T. Fiorino, S. N. Long, M. J. Houle, C. A. Rice, Z. P. Manning, M. J. Krizo, D. W. Bunch, and L. E. Gravley, "Methodology for comparing worldwide performance of diverse weight-constrained high energy laser systems," *Proc. SPIE* **5792**, 76-87 (2005) [doi:10.1117/12.603384].
- [2] S. T. Fiorino, R. J. Bartell, M. J. Krizo, D. J. Fedyk, K. P. Moore, T. R. Harris, S. J. Cusumano, R. Richmond, and M. J. Gebhardt, "Worldwide assessments of laser radar tactical scenario performance variability for diverse low altitude atmospheric conditions at 1.0642  $\mu\text{m}$  and 1.557  $\mu\text{m}$ ," *J. Appl. Rem. Sens.* **3**, 033521 (2009) [doi:10.1117/1.3122349].
- [3] S. T. Fiorino, R. J. Bartell, G. P. Perram, D. W. Bunch, L. E. Gravley, C. A. Rice, Z. P. Manning, and M. J. Krizo, "The HELEEOS atmospheric effects package: a probabilistic method for evaluating uncertainty in low-altitude high energy laser effectiveness," *J. Dir. Energy* **1**(4), 347-360. (2006).
- [4] L. E. Gravley, S. T. Fiorino, R. J. Bartell, G. P. Perram, M. J. Krizo, and K. Le, "Comparison of climatological optical turbulence profiles to standard, statistical, and numerical models using HELEEOS", *J. Dir. Energy* **3**(1), 347-362 (2007).
- [5] G. W. Kamerman, "Laser radar", in *Active Electro-Optical Systems*, pp. 1-76, C.S. Fox, Ed., The Infrared and Electro-Optical Systems Handbook, Vol. **6**, SPIE Optical Engineering Press, Bellingham, WA, (1993).
- [6] G. W. Stimson, *Introduction to airborne radar*, Hughes Aircraft Company, El Segundo, CA (1983).
- [7] S. T. Fiorino, R. J. Bartell, M. J. Krizo, and S. J. Cusumano, "Expected worldwide, low-altitude laser performance in the presence of common atmospheric obscurants," *J. Dir. Energy* **2**(4), 363-375 (2007).
- [8] R. K. Crane and D. W. Blood, "Handbook for the estimation of microwave propagation effects—link calculations for earth-space paths" *Tech. Report P-7376-TR1*, 80 pp., Environmental Research and Technology, Inc, Concord, MA (1979).

**Steven T. Fiorino**, Lt Col, USAF, is an Assistant Professor of Atmospheric Physics at the Air Force Institute of Technology (AFIT). He has B.S. degrees in Geography and Meteorology from Ohio State (1987) and Florida State (1989) universities, an M.S. in Atmospheric Dynamics from Ohio State (1993) and a Ph.D. in Physical Meteorology from Florida State (2002). His research interests include microwave remote sensing, development of weather signal processing algorithms, and atmospheric effects on military weapon systems.

**Richard J. Bartell** received his B.S. degree in Physics from the United States Air Force Academy as a distinguished graduate in 1979. He received his M.S. degree from the Optical Sciences Center, University of Arizona, in 1987. He is currently a Research Physicist with the Air Force Institute of Technology's Center for Directed Energy, where he leads development of the High Energy Laser End-to-End Operational Simulation (HELEEOS) model.

**Matthew J. Krizo** received his M.S.E.E. from the University of Dayton in 2008 and his B.S.E.E. from Cedarville University in 2005. He is currently a Research Engineer with the Center for Directed Energy at the Air Force Institute of Technology, Wright Patterson AFB, Ohio. He is primarily responsible for software development of HELEEOS.

**Gregory L. Caylor** was a research intern with the Center for Directed Energy. He graduated from the University of Dayton in 2008 with a B.S. degree in Mechanical Engineering. He is currently attending United States Air Force pilot training.

**Kenneth P. Moore** was a research engineer with the Center for Directed Energy. He graduated from Cedarville University in 2007 with a B.S. Physics and is currently a PhD student at Ohio University.

**Thomas R. Harris** was a student research assistant with the Center for Directed Energy. He graduated from Cedarville University in 2008 with a B.S. Physics and is currently a graduate student at the Air Force Institute of Technology.

**Salvatore J. Cusumano** is the Director of the Center for Directed Energy located at AFIT. He received his Ph.D. in Control Theory from the University of Illinois in 1988, an M.S.E.E. from the Air Force Institute of Technology in 1977, and a B.S.E.E. from the United States Air Force Academy in 1971. The Center collaborates on directed energy research topics, both high power microwaves (HPM) and high energy lasers (HEL), throughout the DoD community. Dr. Cusumano's research interests span his 25 years of experience in directed energy and include resonator alignment and stabilization, intra-cavity adaptive optics, phased arrays, telescope control, pointing and tracking, adaptive optics and component technology for directed energy. He holds two patents (jointly) for his work in phased arrays.